PHYSICAL REVIEW D

PARTICLES AND FIELDS

THIRD SERIES, VOLUME 33, NUMBER 1 1 JANUARY 1986

Lifetimes, cross sections, and production mechanisms of charmed particles produced by 20-GeV photons

K. Abe,[g] R. Armenteros,[f,*] T. C. Bacon,[c] J. Ballam,[f] H. H. Bingham,[i] J. E. Brau,[j] K. Braune,[f] D. Brick,[b] W. M. Bugg,[j] J. M. Butler,[f] W. Cameron,[c] H. O. Cohn,[d] D. C. Colley,[a] G. T. Condo,[j] P. Dingus,[i] R. Erickson,[f] R. C. Field,[f] B. Franek,[e] R. Gearhart,[f] T. Glanzman,[f] I. M. Godfrey,[c] J. J. Goldberg,[f,†] G. Hall,[c] E. R. Hancock,[e] H. J. Hargis,[j] E. L. Hart,[j] M. J. Harwin,[c] K. Hasegawa,[g] M. Jobes,[a] T. Kafka,[h] G. E. Kalmus,[e] D. P. Kelsey,[e,*] T. Kitagaki,[g] W. A. Mann,[h] R. Merenyi,[h,‡] R. Milburn,[h] K. C. Moffeit,[f] J. J. Murray,[f] A. Napier,[h] V. R. O'Dell,[b] P. Rankin,[f] H. Sagawa,[g] J. Schneps,[h] S. J. Sewell,[e] J. Shank,[i] A. M. Shapiro,[b] J. Shimony,[j] K. Tamai,[g] S. Tanaka,[g] D. A. Waide,[a] M. Widgoff,[b] S. Wolbers,[i,§] C. A. Woods,[c,**] A. Yamaguchi,[g] G. P. Yost,[i] and H. Yuta[g]

[a]*Birmingham University, Birmingham, B15 2TT, United Kingdom*

[b]*Brown University, Providence, Rhode Island 02912*

[c]*Imperial College, London, SW7 2BZ, United Kingdom*

[d] *Oak Ridge National Laboratory, Oak Ridge, Tennessee 37830*

[e]*Rutherford Appleton Laboratory, Chilton, Didcot, Oxon OX11 0QX, United Kingdom*

[f]*Stanford Linear Accelerator Center, Stanford University, Stanford, California 94305*

[g]*Tohoku University, Sendai 980, Japan*

[h]*Tufts University, Medford, Massachusetts 02155*

[i]*University of California, Berkeley, California 94720*

[j]*University of Tennessee, Knoxville, Tennessee 37996*

(SLAC Hybrid Facility Photon Collaboration)

(Received 8 July 1985)

Seventy-one events containing charmed-particle decays have been observed in an experiment using the SLAC Hybrid Facility exposed to a backward-scattered photon beam. Several improvements were made to the apparatus since the previous experiment on charm photoproduction. Results for the charmed-meson lifetimes are consistent with the published results from the previous experiment and the two data samples have been combined yielding a total sample of 136 charm events. After imposing rigorous cuts, 50 neutral, 48 charged, and 2 charged/neutral ambiguous decays remain. From these, the charmed-meson lifetimes are measured to be $\tau_{D^\pm}=(8.6\pm1.3^{+0.7}_{-0.3})\times10^{-13}$ sec, $\tau_{D^0}=(6.1\pm0.9\pm0.3)\times10^{-13}$ sec, and their ratio $\tau_{D^\pm}/\tau_{D^0}=1.4\pm0.3^{+0.2}_{-0.1}$. The total charm cross section at a photon energy of 20 GeV has been measured to be $(62\pm8^{+15}_{-10})$ nb. There is evidence for both $D\bar{D}X$ and $\bar{D}\Lambda_c^+X$ production with $\sigma_{\bar{D}\Lambda_c^+X}/\sigma_{\text{charm}}=(71\pm11\pm6)\%$.

I. INTRODUCTION

The SLAC Hybrid Facility (SHF) Photon Collaboration has previously published results from an experiment (BC72/73) to study the production and decay of charmed particles.[1] Data and results obtained by combining events from this experiment with those from a new experiment (BC75) incorporating some improvements to the apparatus are presented.

Charmed-particle lifetimes and their ratios provide experimental tests of decay-mechanism models. The first predictions[2] of charmed-particle lifetimes were made by treating the heavy charmed quark as a free particle. Thus, the decays of charmed mesons could be described by the decay of the charmed quark with the light constituents of the mesons acting as passive spectators. This spectator decay mechanism, shown in Fig. 1(a), predicts equal lifetimes for the charged and neutral D mesons. Early experiments,[3] however, found the D^0 lifetime (τ_{D^0}) to be much smaller than $\tau_{D^\pm}$, favoring the dominance of decay mechanisms involving more than one constituent of the D meson,[4] such as the exchange mechanism [see Fig. 1(b)]. In BC72/73, the charged- and neutral-D lifetimes were measured and their ratio found[1] to be $\tau_{D^\pm}/\tau_{D^0}=1.1^{+0.6}_{-0.3}$. This suggested that the spectator-

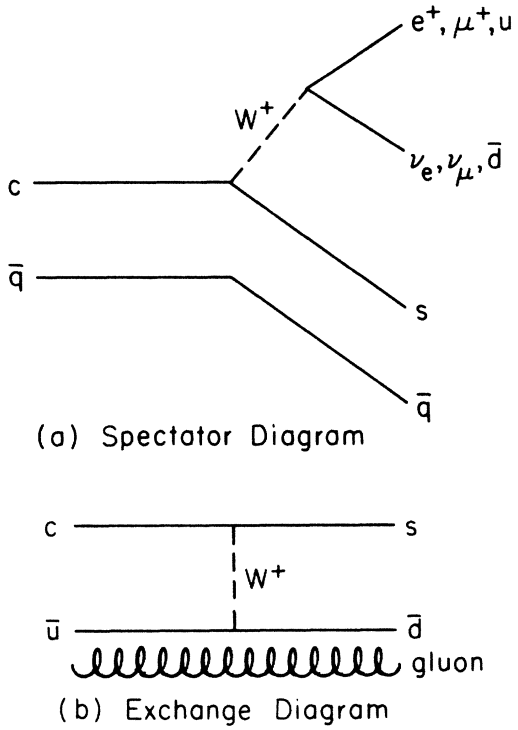

FIG. 1. Cabibbo-angle-favored D-meson decay diagrams for the (a) spectator, and (b) exchange mechanisms.

decay mechanism in D^0 decay is more important than was previously thought.

Using the combined data from the two experiments, the total charmed-particle photoproduction cross section has been measured and compared with the predictions[5] of various models. The separate contributions of associated (baryon-antimeson) and pair (meson-antimeson) production have been measured, as well as the fraction of D mesons produced via D^* decays.

Approximately 1.2×10^6 pictures containing 310000 hadronic interactions were taken in the new experiment. Seventy-one events were found to have direct visual evidence for the production and multiprong decay of at least one charmed particle. The 65 events found in the previous experiment were reviewed and treated in the same way as those found in the new experiment. Since the conditions of the two experiments were very similar and the data found to be consistent, the data from BC72/73 and BC75 were combined and the final results for the two experiments are presented. The 136 events from the combined experiments contain 161 visible multiprong decays of charmed particles. Stringent cuts were imposed on the data to ensure that the efficiency for finding the decays used in the analysis was high and uniform; 100 decays from 94 events passed these cuts.

Both experiments used a 20-GeV backward-scattered photon beam which passed through the SLAC 1-m bubble chamber where the normal 3-view stereo camera was supplemented with a high-resolution camera allowing efficient detection of charmed-particle decays. Downstream detectors were used to trigger the cameras on the occurrence of hadronic interactions in the bubble chamber.

The energy of the photon beam was sufficiently far above the charm threshold to yield a useful number of events but low enough to give events with a small average charged-particle multiplicity, so that in the region close to the production vertex decays are clearly visible.

An important feature of these results is that the detector efficiency for decays close to the production vertex was measured using multiple scans. These measurements were confirmed using the relatively large numbers of neutral-strange-particle decays seen in the film.

The experimental details are described in Sec. II. Section III gives the analysis and results on the lifetimes of charged and neutral D mesons, production mechanisms, and production cross sections. Finally, Sec. IV contains the conclusions.

II. EXPERIMENTAL DETAILS

The experiment was performed at the SLAC Hybrid Facility (Fig. 2). The beam, bubble chamber, downstream detectors, trigger, and data acquisition system are described in detail in Ref. 1 and references therein.

The 20-GeV photon beam was produced by backscattering laser light from 30-GeV electrons provided by the SLAC linear accelerator. The photon-beam spectrum had a central value of 19.6 GeV and a full width at half maximum (FWHM) of 2 GeV. The beam intensity was 20—30 γ's per pulse at a rate of 10—12 Hz and the beam had a circular cross section of 3 mm in diameter when traversing the bubble chamber.

The downstream detector system consisted of three sets (four in BC72/73) of proportional wire chambers (PWC's), two atmospheric-pressure Cherenkov counters, and an array of lead-glass blocks. These detectors were made insensitive to particles in a narrow region perpendicular to the bubble-chamber magnetic field which contained the beam and most of the background e^+e^- pairs.

The camera flash lamps were triggered when sufficient energy was deposited in the lead-glass blocks or a track which appeared to originate in the fiducial volume of the bubble chamber was detected in the PWC's.

A. Improvements

The basic experimental apparatus had been in use at the SHF since data taking began for BC72/73. However, during four years of operation with about four months of

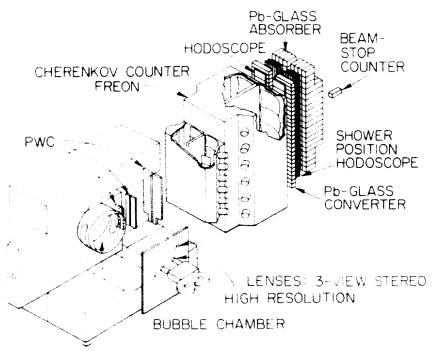

FIG. 2. The SLAC Hybrid Facility with bubble chamber, proportional wire chambers, Cherenkov counters, lead-glass columns, and beam-stop counter.

data taking per year, several changes, primarily aimed at improving the photographic resolution, were made. The significant improvements are described below.

1. The bubble chamber

Toward the end of BC72/73 the glass window through which the events were photographed was replaced. The new, thicker window extended a further 82 mm into the chamber, forcing bubbles from the sealing gasket to flow around the window rather than across the field of view. The reduced optical path through the hydrogen resulted in less optical distortion; and the smaller liquid-hydrogen volume allowed for better control of the chamber operating conditions. A further improvement was made during the course of BC75 by replacing the hydrogen cooling system by a deuterium one. The chamber was operated at a temperature near 29 K with a large expansion ratio giving a high bubble density of about 60 bubbles/cm and a slow bubble growth rate, thereby allowing sufficient time for the camera trigger.

2. The high-resolution camera

A new high-resolution camera was installed[6] in which the single 360-mm Schneider Componon S lens used previously was replaced by a pair of Nikon Apo-Nikkor 610-mm lenses. The two lenses each recorded about half the usual beam path, with a small overlap between the images. The new camera gave a resolvable point separation close to the Rayleigh criterion of about 30 μm for a depth of field of ± 2 mm. To realize this resolution away from the optic axis, it was necessary to filter the light, thereby reducing chromatic aberrations. This in turn required the use of condenser lenses. The optic axis of each lens was 6.7 cm above the photon-beam axis and perpendicular to the surface of the bubble-chamber window. As a result, the direct specular reflections of the flash tubes from the glass and piston surfaces did not obscure the beam region.

In order to take advantage of the improved resolution, smaller bubbles (about 40 μm diameter) were produced after a reduced flash delay and photographed with a flash of shorter duration. This shorter flash pulse was achieved with the use of improved flash lamps, a power supply with reduced capacitance, and a faster triggering pulse.

3. The camera trigger

The reduction in the flash delay required that the time for the trigger decision be reduced. The track information from the PWC's was part of this trigger. Previously, a software algorithm reconstructed particle trajectories projected onto the nonbend plane, triggering only on those events containing at least one such trajectory crossing the fiducial volume. The reduction in this decision time was achieved by substituting a dedicated hardware processor[7] for the software algorithm.

4. The Cherenkov counters

The Cherenkov counters contained Freon 114 at one atmosphere during BC75. This reduced the pion threshold from 3.2 GeV/c in BC72/73 in which Freon 12 was used, to about 2.6 GeV/c.

B. Event selection

The results presented here are based on combined data from the two experiments (Table I). In BC75 the film was first scanned for hadronic events. Each event was then closely examined, using the high-resolution film at high magnification, for decays occurring within 1.5 cm of the production vertex.

An event was retained for further analysis if either a decay point was visible or any of the tracks when extrapolated back missed the production vertex by a distance greater than one track width. Charge balance was invoked to distinguish secondary interactions from decays. These events were then subjected to a number of cuts. The purpose of the first set of cuts was to remove noncharm decays, specifically strange-particle decays and γ conversions. The following were rejected: (i) decays with fewer than two charged tracks; (ii) two-prong decays consistent with photon conversions or strange-particle decays ($m_{e^+e^-} < 50$ MeV/c^2, $m_{\pi^+\pi^-} < 550$ MeV/c^2, $m_{p\pi} < 1130$ MeV/c^2, or m within 5σ of γ, K^0, or Λ mass); and (iii) three-prong decays consistent with charged-strange-particle decays or neutral-strange-particle decays superimposed on a track from the production vertex.

Within the fiducial volume, a total of 136 events remained containing 161 visible multiprong charm decays. An example of such an event is shown in Fig. 3. High-magnification (at least 20 times space) photographic prints were made from which the projected decay lengths and impact distances were measured. The impact distance for a track from a decay is defined in the film plane as the perpendicular distance from the extrapolation of the track to the primary vertex. For any decay, the largest impact distance was called $d_{\max}$ and the second largest d_2 (see Fig. 3 inset).

To ensure that events were detected with high and uniform efficiency and to reduce topological ambiguity it was further required for each decay that (iv) $d_{\max}$ be greater than 110 μm (2–3 track widths) ensuring that the scanning efficiency was high and independent of overall event topology, (v) d_2 be greater than 40 μm ensuring that the decay was multipronged, and (vi) the projected decay length (l) be greater than $l_0 = 0.6$ mm, reducing the number of charged/neutral ambiguous decays in the sample by separating the decay from the region where the density of tracks from the primary vertex was highest.

Figure 4 shows that although the number of decays decreases gradually with increasing l_0, the fraction of ambi-

TABLE I. Details of the experiment.

	BC72/73	BC75	Combined
Number of pictures taken	2 408 000	1 225 000	3 633 000
Hadronic events in fiducial volume	378 000	310 000	688 000
Events containing charm	65	71	136

FIG. 3. Photograph of event taken by high-resolution camera. The inset shows a sketch of the maximum projected impact distance (d_{max}), and second largest projected impact distance (d_2) used in the analysis.

guous decays decreases rapidly between l_0 values of 0.5 and 0.6 mm. A cut of 0.5 mm was used for BC72/73; however, the increased statistics show that $l_0=0.6$ mm is preferred.

After imposing the above cuts, 13 decays remained topologically charged/neutral ambiguous. The most frequent ambiguity was between a charged-decay candidate and a neutral candidate superimposed upon a track originating from the primary vertex. In five cases, only one topological interpretation had an invariant mass less than 2σ above the D-meson mass and it was accepted as such. It should be noted that no unambiguous charged or neutral decay failed this criterion. Of the remaining eight topologically ambiguous decays, three had an interpretation compatible with a Cabibbo-angle-favored D-meson decay into a charged final state with no undetected neutrals which pointed back to the primary vertex and were resolved on this basis. Of the remaining five decays, three were $D^{*\pm}\to D^0\pi^\pm$ candidates with a minimum mass difference between the $D^0\pi^\pm$ system and the D^0 of less than 160 MeV/c^2. These were resolved as neutral decays. In order to demonstrate that this was reasonable the topologically unambiguous decays were examined using the same criterion and it was found that there were an additional nine $D^{*\pm}\to\pi^\pm D^0$ candidates in the neutral decays while the charged sample had only one decay with a minimum mass difference less than 160 MeV/c^2. For the charged decays no signal is expected because $D^{*0}\to\pi^- D^+$ is not allowed. Section III C 4 describes the D^* evidence in more detail. Two decays remained unresolved, and these were ambiguous between two-prong and three-prong interpretions. In one decay, the three-prong decay was positive and in the other it was negative. Their projected decay lengths were 1.32 and 1.95 mm.

Figure 5 shows a scatter plot of d_{max} versus projected decay length for all decays. Decays with $d_2<40$ μm and the region excluded by the cuts are indicated. These data points illustrate that the cuts have been placed well into a smoothly varying distribution containing many decays below the cuts.

After all the cuts were applied 100 charm decays remained. Of these, 50 are neutral, 48 are charged, and 2 are charged/neutral ambiguous decays. These decays are from 94 events.

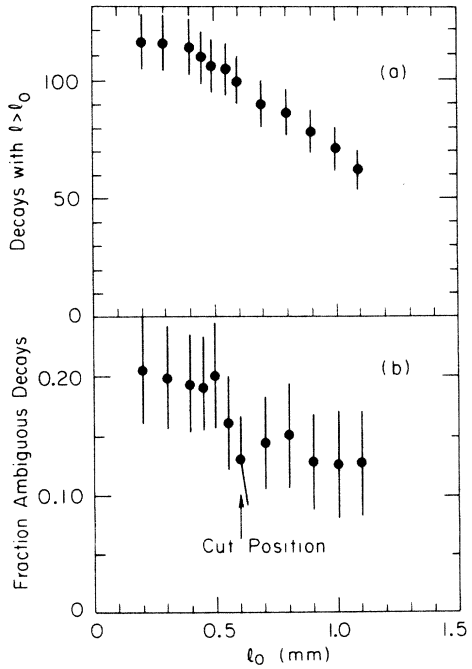

FIG. 4. (a) Number of decays and (b) fraction of topologically ambiguous decays as a function of the projected decay length cut l_0. Data sample has the $d_{max}>110$ μm and $d_2>40$ μm requirement on each decay.

C. Scanning and triggering efficiencies and sensitivity

1. *The scanning efficiency*

All of the film was scanned twice and 43% of the BC75 film was scanned more than twice for events containing

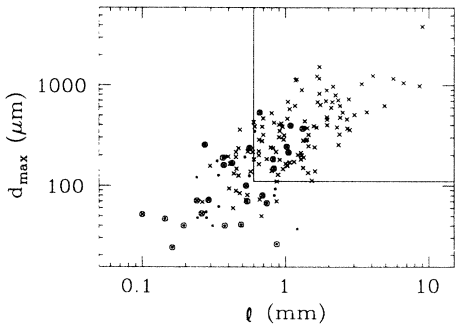

FIG. 5. Scatter plot of d_{max} against projected decay length (l) for all multiprong decays. The region of the plot excluded by the cuts is also indicated. Decays with $d_2>40$ μm are denoted by $\times$ and decays with $d_2\leq 40$ μm by $\bullet$. In addition, if a decay is the shorter decay in an event containing two visible multiprong decays then its symbol is surrounded by a circle.

decays close to the production vertex. The efficiencies for finding such events were calculated using a maximum-likelihood method.[8] The logarithmic likelihood is given by

$$L=\left[\sum_{i=1}^{n} N_i\right]\ln\epsilon+\left[\sum_{i=1}^{n}(N-N_i)\right]\ln(1-\epsilon)$$
$$-N\ln[1-(1-\epsilon)^n],$$

where N is the total number of events found, N_i is the number of events found on scan i, and n scans were performed. The single-scan efficiency ϵ was then determined by maximizing L. The most important advantage of this method over the standard Geiger-Werner method[9] is that it can be extended to any number of scans. The combined scanning efficiency for finding charm events passing cuts was calculated to be $(97^{+2}_{-4})\%$.

Figure 6 shows the efficiency for finding decays as a function of projected decay length. Only decays with $d_{\max}>110$ μm and $d_2>40$ μm were used. Charm and neutral-strange-particle decays are shown separately. The scanning efficiency is seen to be high and uniform for all regions near and above the cuts.

As an independent check of the efficiency for detecting decays close to the primary vertex, the decay lengths and impact distances were also studied for neutral-strange-particle decays of K^0's and Λ's. Only decays with $d_2<700$ μm were used, as these have great visual similarity to neutral-D decays into two charged particles. Figure 7 shows the projected decay length and impact distance distributions for the combined K^0 and Λ samples. A Monte Carlo method using information from the large number of observed K^0 and Λ decays at longer distances was used to predict the shapes of these distributions which are shown as curves on Fig. 7.

In both the data and the Monte Carlo samples shown in Fig. 7(a), K^0's and Λ's with $d_{\max}<110$ μm were eliminated so that the detection efficiency at small decay lengths could be examined independently of that for $d_{\max}$. The Monte Carlo sample was normalized to the data for $l>0.6$ mm. Even below the cuts the data are consistent with the levels predicted by the Monte Carlo simulation, indicating that the efficiency remains constant. Figure 7(b) shows the corresponding plot of $d_{\max}$ for K^0's and Λ's with $l>0.6$ mm. Note that the first two points cover the range $0<d_{\max}<110$ μm.

Comparing the published[10] inclusive K^0 and Λ cross section, $\sigma_{(K^0+\Lambda)}=15.0\pm0.4$ μb, to the cross section calculated using K^0 and Λ decays found on the charm scan with a projected decay length less than 1.5 cm, $\sigma_{(K^0+\Lambda)}=14.6\pm1.5$ μb, confirms the high scanning efficiency within this region. These cross sections and the distributions of projected decay length and impact parameters show that the scanning efficiency for short neutral decays

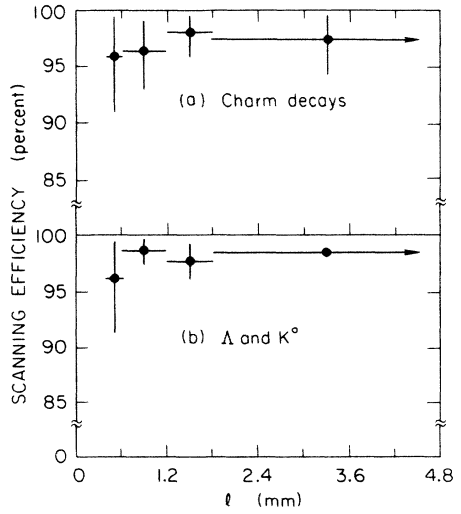

FIG. 6. Dependence of the scanning efficiency on the projected decay length l for (a) charm decays and (b) Λ and K^0 decays found on the charm scan.

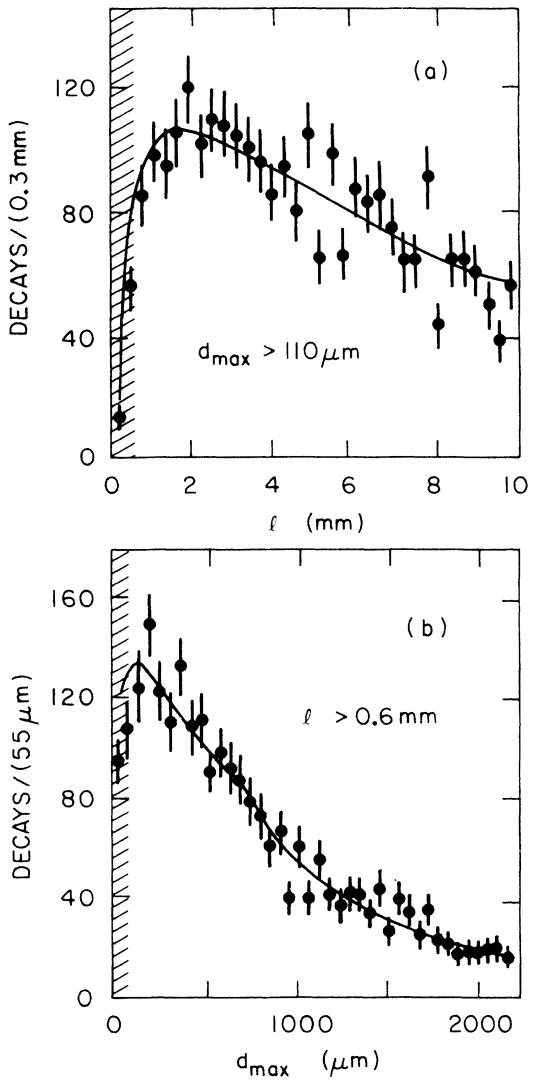

FIG. 7. Neutral-strange-particle decays (K^0,Λ) found in the scan for charm events (a) projected-decay-length l distribution, and (b) maximum-impact-distance $d_{\max}$ distribution. The curves show the expected distributions. The shaded area indicates the region below the cuts used in the charm-decay analysis.

into two charged particles passing the cuts is high and uniform.

2. The trigger efficiency

The trigger efficiency for hadronic events was determined by taking every 50th frame of film untriggered while still recording the trigger decision. From these data the trigger efficiency for hadronic events was determined as a function of the number of charged particles in the event. The trigger efficiency for charmed-particle events was calculated by assuming the events containing charm and other hadronic events of the same charged multiplicity have equal efficiency. It was found that the efficiency was high and uniform for charged multiplicities greater than three. Taking into account the small variations in the configuration of the downstream detectors for different running periods, the weighted average charm trigger efficiencies for BC72/73 and BC75 were $(87\pm4)\%$ and $(85\pm5)\%$, respectively. These values were checked by a Monte Carlo calculation in which each of the charm events was redistributed in the fiducial volume and rotated about the beam direction. The trajectories of the produced particles were then extrapolated into the downstream detectors yielding a trigger efficiency of $(90\pm10)\%$.

3. The sensitivity

The sensitivity of the experiment expressed in events produced per unit cross section was determined from the total photon path length in the hydrogen and the scanning and triggering efficiencies. The number of photons in the experiment was measured by summing the counts from the beam-stop counter (see Ref. 1) for all beam pulses for which the camera was ready to trigger. The counter was calibrated by counting e^+e^- pairs observed in the bubble chamber and those collected by the pair spectrometer. The sensitivity for charm events was found to be (5.4 ± 0.4) events/nb for the combined experiments. This sensitivity was also calculated by comparing the total number of hadronic interactions found to the known total hadronic cross section, and correcting for the differences in the charm and hadronic scanning and triggering efficiencies. The values found by these two methods were consistent.

D. Background

Four approaches were used to estimate the background to the charm signal.

(i) A direct measurement of the background was made by scanning a region of the film just beyond that populated by the charmed particles. 45% of all hadronic events were searched for decays out to 15 mm from the production vertex, 33% to 30 mm, and 22% only to 10 mm. No charm-decay candidates were found beyond 10 mm from the production vertex. This yielded an upper limit on the number of background events from all sources simulating charmed-particle decays of less than 3.1 events (90% confidence level). The calculation allowed for the fact that some sources of background are not independent of the distance from the production vertex.

(ii) Calculations were made of the possible contributions to the charm signal from various specific background sources. Extensive Monte Carlo calculations showed that the cuts imposed on the two-body invariant masses (see Sec. II B) were sufficient to ensure that a very small number of the two-prong decay candidates could have come from K^0 or Λ decays. The background from two-body K^0 and Λ decays is concentrated at low dipion effective-mass values (just above the 550-MeV/c^2 cut) and was calculated to contribute <0.4 decays to the entire experiment. This number includes the effect of misfitted K^0 and Λ decay tracks which scattered elastically or underwent one-prong decays. Three-body Λ decays ($\Lambda\rightarrow pe\bar{\nu}$) comprised the largest single background but were calculated to contribute less than 0.5 decays.

Another type of potentially significant background was that due to the secondary interaction of a particle emitted from the primary vertex producing a low-momentum (<60 MeV/c) unseen proton. Such an interaction would have the charge configuration of a decay. The size of this background was calculated using published experimental data on cross sections, invariant mass, and momentum-transfer distributions as a function of charged multiplicity. The contributions from this source were found to be negligible except for two- and three-prong final states with undetected neutral(s), for which the estimated backgrounds were found to be 0.2 and 0.1 decays, respectively.

(iii) Each of the charm-decay candidates passing cuts was examined to determine if it could be due to a secondary interaction of a particle emitted from the primary vertex, as discussed above. The recoil proton momentum was calculated for each candidate assuming that it came from a peripheral secondary interaction with a proton (i.e., $\pi^+p\rightarrow pX^+$, where X^+ is the observed charm-decay candidate and the π^+ momentum being defined as the vector sum of the visible decay products). Only two three-prong events of the 48 charged-decay candidates could have had an invisible recoil proton. Both of the events containing these decays also contain a second visible decay vertex, thus making the charm interpretation very probable. In addition, both of the decays have a large-transverse-momentum imbalance with respect to their lines of flight which is inconsistent with this background explanation. Only three two-prong events of the 50 neutral-decay candidates could have had an unseen recoil proton and one of these has a large-transverse-momentum imbalance.

(iv) Backgrounds due to other sources such as two independent γp interactions close together, or secondary interactions with deuterons present in the liquid hydrogen were calculated and found to be negligible.

In conclusion, these observations and calculations indicate that very few, if any, of the charm decays are due to background.

III. RESULTS

A. Event characteristics

The 100 charm decays which remained after cuts are summarized in Table II. These are 50 neutral, 15 positive,

TABLE II. Details of events with at least one decay passing decay selection.

	BC72/73	BC75	Combined	
Number of events	50	44	94	
Number of decays	53	47	100	
Positive decays				
Three-prong	8	7	15	
Five-prong	0	0	0	
Negative decays				48
Three-prong	16	15	31	
Five-prong	2	0	2	
Neutral decays				
Two-prong	13	8	21	
Four-prong	13	16	29	50
Charged/neutral ambiguous	1	1	2	

33 negative, and 2 charged/neutral ambiguous decays. The $d_{\max}$, d_2, l, $p_{\rm vis}$, and $m^{\pi}_{\rm vis}$ distributions are shown in Figs. 8–10. The visible momentum $p_{\rm vis}$ is the vector sum of charged-particle momenta observed in the decay and $m^{\pi}_{\rm vis}$ is the invariant mass of the charged-decay particles assuming they are all pions. While there are only six events having both decays passing all the cuts of Sec. II B, a further 39 events have visual evidence for a second charm vertex (including one-prong decays). The second vertices were found with very high efficiency well below the standard cuts because the 94 events were examined in great detail.

1. Evidence for D-meson decays

A search was made for D decays into final states with no undetected neutrals. The following conditions were also imposed.

(i) Only decays into Cabibbo-angle-allowed final states consistent with particle identification were permitted.

(ii) The reconstructed momentum vector of the decaying particle was required to match within 3 standard deviations its direction as measured in the film plane (the typical measurement error in this direction was 20 mrad).

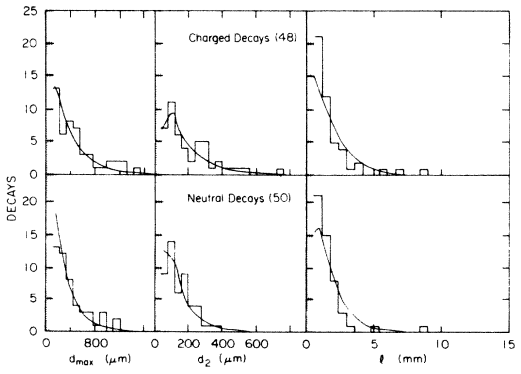

FIG. 8. Distribution of $d_{\max}$, d_2, and l. The shaded area indicates the region below the cuts. The curves were obtained using $\tau_{D^0}=6.1\times10^{-13}$ sec, $\tau_{D^\pm}=8.6\times10^{-13}$ sec and a Monte Carlo calculation (see Appendix A).

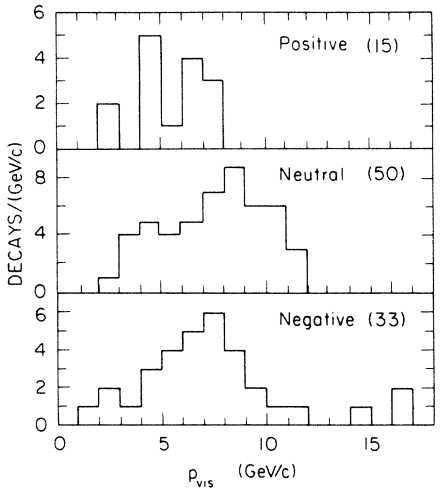

FIG. 9. Visible momentum distribution for positive-, neutral-, and negative-charmed-particle decays; mean values are 5.4, 7.5, and 7.5 GeV/c, respectively.

(iii) The error in the effective mass was required to be less than 30 MeV/c^2.

Figure 11 shows the distributions for all mass contributions satisfying these conditions. A signal at the D mass [$m_{D^\pm}=1869$ MeV/c^2, $m_{D^0}=1865$ MeV/c^2 (Ref. 11)] stands out clearly for the charged decays. The signal for the neutral decays is less clear because there are 112 mass combinations for the 36 neutral decays while there are only 40 mass combinations among the 32 charged decays. A smaller combinatorial background occurs in the $D^\pm$ sample because tracks of the same charge as the decaying particle were not tried as kaons. In the neutral sample, a charged particle of either sign could be a kaon.

Fully reconstructed decays were defined as those satisfying conditions (i), (ii), and (iii) above, and having an ef-

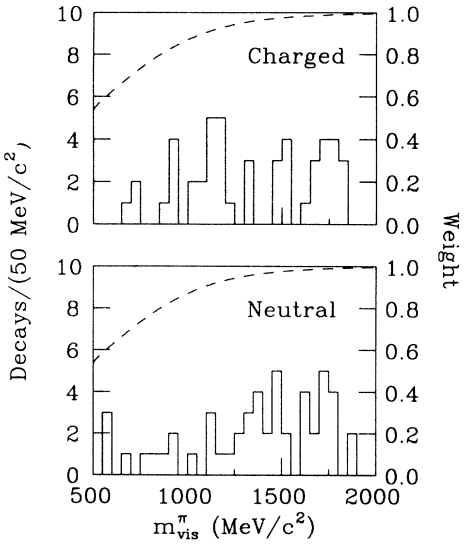

FIG. 10. Distribution of $m^{\pi}_{\rm vis}$ for the charged and neutral decays. The dashed curves show the dependence of the weight used in the determination of the mean lifetimes (see text) on $m^{\pi}_{\rm vis}$ as calculated by Monte Carlo simulation (see Appendix A).

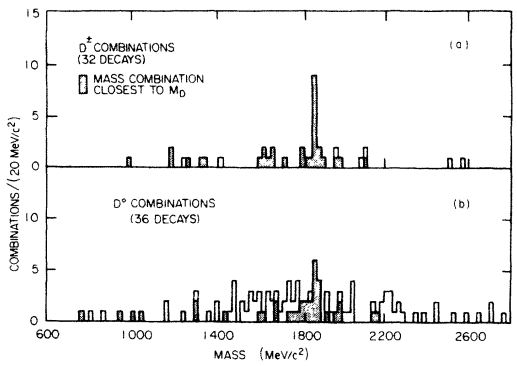

FIG. 11. Invariant-mass distribution for Cabibbo-angle-favored decays of (a) $D^{\pm}$, and (b) D^0. All decays pointing to the primary vertex including those containing one reconstructed π^0 or a visible K_S^0 are included. Particle-identification information has been used. The error on the mass was required to be less than 30 MeV/c^2 for a combination to be included. The decays producing the combinations above m_D are all consistent with the D mass when particle mass assignments are changed. The shaded entries show the mass combination closest to m_D for each decay.

fective mass within 3.5 standard deviations of the D mass. 15 charged and 16 neutral decays were selected on this basis. 12 of these contain identified kaons (10 $K^{\pm}$ and 2 K_S^0). The number of these fully reconstructed D decays is consistent with the known branching ratios.[11]

2. Search for $F^{\pm}$ decays

A similar invariant-mass plot for the charged decays tried as $F^{\pm}$ candidates is presented in Fig. 12. It can be seen that the enhancement near 2040 MeV/c^2 is due to the reflection of the D meson when one of the decay pions is assigned a kaon mass, as no accumulation remains (shaded region of plot) once the fully reconstructed D decays are removed from the sample. No significant peak is observed at the reported F mass[11] of 1971 MeV/c^2. In addition, a plot of $M_{K^+K^-}$ for all two-particle combinations in the charm events, consistent with particle identification, shows no signal near the ϕ mass. Such a signal would be expected if the charm events included a substantial fraction of $F^{\pm}\to\phi X^{\pm}$ decays.

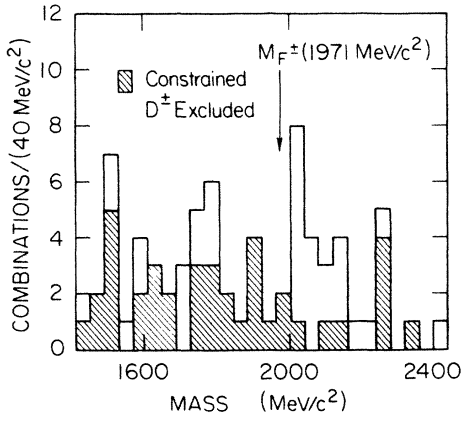

FIG. 12. Invariant-mass distribution for charged decays interpreted as Cabibbo-angle-favored decays of $F^{\pm}$ (all pion final states were tried). Only decays which point to the primary vertex are included. Particle-identification information has been used. The hatched histogram shows those combinations remaining after decays interpreted as fully reconstructed D decays were removed. The enhancement at 2040 MeV/c^2 is a reflection of D decays when a pion is assigned the kaon mass.

3. Search for Λ_c^+ decays

No fully reconstructed Λ_c^+ decays were found in the sample of positive decays passing cuts, and no Λ's or $\Sigma^{\pm}$'s were found in the events containing these positive decays. All mass combinations consistent with Cabibbo-angle-favored Λ_c^+ decays were examined both at positive decay vertices and at primary vertices. These showed no signal above the combinatorial background at the reported Λ_c^+ mass[11] of 2282 MeV/c^2.

To summarize, all 100 decays are compatible with the D-meson hypothesis. There is evidence for fully reconstructed Cabibbo-angle-allowed D decays in both the charged and neutral samples and the fraction of these is consistent with measured D-meson branching ratios.

B. Lifetimes

The method used to obtain the proper flight time for each decay allowed both fully reconstructed decays and those with undetected neutrals to be used in the calculation of average lifetimes.[12] The influence of possible contributions from Λ_c^+ and $F^{\pm}$ decays to the charged lifetime is discussed. Finally, the results on the $D^{\pm}$ and D^0 lifetimes and their ratio are presented.

1. Method for calculating the proper flight time

The proper flight time t for a D meson traveling a distance l and having a momentum p is

$$t = l\frac{m_D}{c}\frac{1}{p}\ , \tag{1}$$

where m_D is the D-meson mass. To determine the proper flight time of a decay the path length and the momentum are needed.

Because decays occurring close to the production vertex are difficult to see, the decay length in the above formula is replaced by the effective path length, $l_{\rm eff}$. This quantity is defined to be the distance between the decay vertex and l_m, the first point on the flight path at which the decay would pass all the cuts described in Sec. II B (i.e., l_m is the maximum of $[(110\ \mu{\rm m}/d_{\rm max})l]$, $[(40\ \mu{\rm m}/d_2)l]$, or 0.6 mm):

$$l_{\rm eff} = l - l_m\ .$$

The $l_{\rm eff}$ distribution is presented in Fig. 13. Given that the distribution of t is exponential, l may be replaced with $l_{\rm eff}$ in Eq. (1) since the point at which the decay passes all cuts is independent of the decay point.

The momentum of the D mesons is not completely determined in most cases since there were undetected neutral particles in the decay. However, the quantities $p_{\rm vis}$

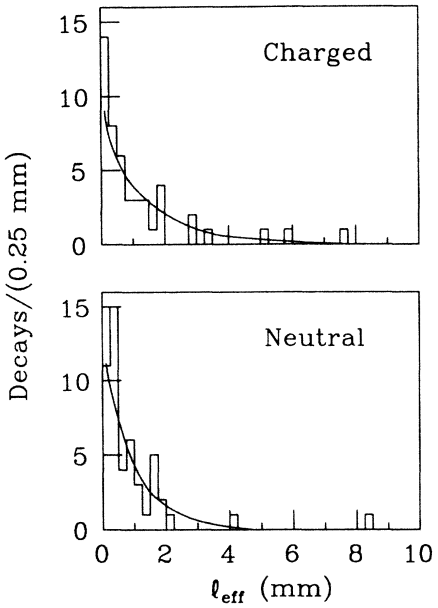

FIG. 13. Distribution of l_{eff} for the charged and neutral decays. The curves were obtained using $\tau_{D^\pm}=8.6\times10^{-13}$ sec, $\tau_{D^0}=6.1\times10^{-13}$ sec, and a Monte Carlo calculation (see Appendix A).

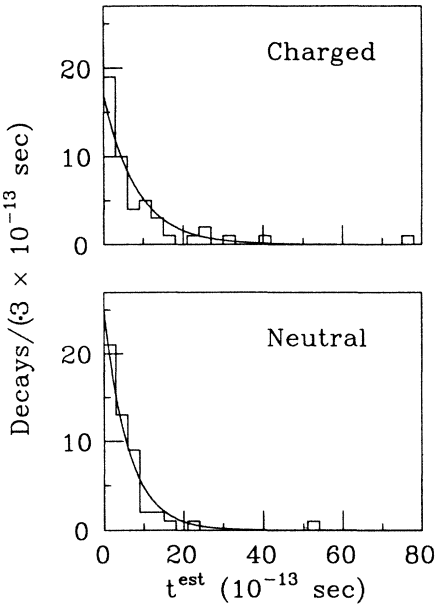

FIG. 14. Distribution of t^{est} (defined in the text) for charged and neutral decays. The curves are exponentials corresponding to the measured lifetimes of $\tau_{D^\pm}=8.6\times10^{-13}$ sec and $\tau_{D^0}=6.1\times10^{-13}$ sec from this experiment.

and m^{π}_{vis} were used to estimate the D momentum according to the formula

$$\left[\frac{1}{p}\right]^{\text{est}}=\alpha\frac{m^{\pi}_{\text{vis}}}{m_D}\frac{1}{p_{\text{vis}}}\ .$$

All decays, whether fully reconstructed or not, were treated in this way. The constant α was determined by a Monte Carlo calculation (see Appendix A). The generated D decays from the Monte Carlo were treated in the same way as the real events. Comparing the average value $(1/p)$ of the generated D decays with the average value of $(1/p)^{\text{est}}$, α was found to be 1.10 ± 0.02. The error in α arises from the uncertainties in the D-meson branching ratios. The deviation of α from unity is largely because all charged-decay tracks were assumed to be pions. The value was found to be insensitive to the specific cuts used in this experiment and essentially independent of the D-meson momentum and, therefore, of the production model.

The estimated flight time, t^{est}, is obtained by substituting l_{eff} and $(1/p)^{\text{est}}$ for l and $(1/p)$ in Eq. (1):

$$t^{\text{est}}=l_{\text{eff}}\frac{m_D}{c}\left[\frac{1}{p}\right]^{\text{est}}\ .$$

Figure 14 shows the t^{est} distribution for the charged and neutral decays.

The reliability of t^{est} as an estimate of the proper flight time for a given decay can be deduced by examining, by means of the Monte Carlo–generated decays, the standard deviation, σ_y, of the quantity $y=p(1/p)^{\text{est}}$ as a function of m^{π}_{vis}. For m^{π}_{vis} close to the D mass σ_y is small while at low values of m^{π}_{vis} it increases significantly. It can be shown that the standard deviation of the distribution of t^{est} for a given visible mass m^{π}_{vis} is

$$\sigma_{t^{\text{est}}}=\tau(1+2\sigma_y{}^2)^{1/2}\ ,$$

where τ is the mean D lifetime. To account for the fact that the uncertainty in t^{est} depends upon m^{π}_{vis}, each decay was weighted by the factor $(\tau/\sigma_{\text{est}})^2=(1+2\sigma_y{}^2)^{-1}$ which is flight time independent. This weight ω is plotted in Fig. 10 as a function of m^{π}_{vis}. The average weights for the neutral and charged decays are 0.92 and 0.92, respectively.

The mean lifetime was estimated by

$$\tau^{\text{est}}=\frac{\sum_{i=1}^{N}t_i^{\text{est}}\omega_i}{\sum_{i=1}^{N}\omega_i}\ ,$$

where N is the total number of decays.

2. *Lifetime results*

Using the above procedure the weighted mean lifetimes were calculated to be $\tau^{\text{est}}_{\pm}=(8.6\pm1.3)\times10^{-13}$ sec and $\tau^{\text{est}}_{0}=(6.0\pm0.9)\times10^{-13}$ sec for the 48 charged and 50 neutral decays, respectively. Setting all weights to unity had only a small effect on these average values, increasing the charged lifetime by 4% (0.26σ) and leaving the neutral lifetime unchanged.

Separate lifetimes for the two- and four-prong D^0 decays were calculated. The mean lifetime for the four-prong decays was somewhat longer than that obtained from the two-prong events but the two values were compatible with each other. Separate lifetimes were also calculated for the samples of fully reconstructed $D^{\pm}$ and D^0 decays. Although the mean lifetime of the fully reconstructed D^0 decays was longer than the value obtained

from all D^0 decays, the results were compatible. The charged-mean-lifetime values are also consistent. In BC72/73 a maximum-likelihood method was used to calculate the lifetimes. The results of that analysis on the combined data differ by less than 8% (0.53σ) (charged) and 1% (0.07σ) (neutral) from the results presented here.[13]

A correction is required to account for the two charged/neutral ambiguous decays. To estimate this correction, the lifetime calculation was repeated using the four possible interpretations of these two decays. The correction is small, not changing the charged lifetime and increasing the neutral lifetime by 0.1×10^{-13} sec.

The influence of possible contributions from Λ_c^+ and $F^\pm$ production on the charged decay sample is considered below.

(i) Any Λ_c^+ contribution only affects the positive decay sample. The lifetime calculated for this sample is $(9.2^{+2.6}_{-2.4})\times10^{-13}$ sec while for the negative decay sample it is $(8.4\pm1.5)\times10^{-13}$ sec. These two values are fully compatible. The number of Λ_c^+'s in our sample which pass cuts depends on the Λ_c^+ production cross section, momentum distribution, lifetime, and multiprong branching ratio. This number was estimated by a Monte Carlo calculation (see Appendix A) using the production cross section determined in this experiment (see Secs. III C and III D) and a lifetime of[11] 2.3×10^{-13} sec. Only (2 ± 2) Λ_c^+ decays would pass the cuts described in Sec. II B. These assumptions would result in a $D^\pm$ lifetime only $(3\pm3)\%$ (0.2σ) longer than $\tau_\pm^{\rm est}$.

(ii) The effect of $F^\pm$ decays in our sample was estimated by Monte Carlo methods. Using an $F^\pm$ lifetime of[11] 1.9×10^{-13} sec and assuming that F production is 10% of the total charm cross section, the $D^\pm$ lifetime was found to be $(2\pm2)\%$ (0.17σ) longer than $\tau_\pm^{\rm est}$.

Since no evidence was found for Λ_c^+ or $F^\pm$ decays in the charged-decay sample passing cuts, no corrections were made to the central values of the $D^\pm$ lifetime. However, the quoted error on the $D^\pm$ lifetime includes the uncertainty in the contribution of Λ_c^+ or $F^\pm$ decays to $\tau_\pm^{\rm est}$.

The final lifetime results are

$$\tau_{D^\pm}=(8.6\pm1.3^{+0.7}_{-0.3})\times10^{-13}\ \text{sec}\ ,$$

$$\tau_{D^0}=(6.1\pm0.9\pm0.3)\times10^{-13}\ \text{sec}\ .$$

The proper-flight-time distributions corresponding to these mean lifetimes are given by the curves of Fig. 14. These values yield a ratio for the charged/neutral lifetimes of

$$\frac{\tau_{D^\pm}}{\tau_{D^0}}=1.4\pm0.3^{+0.2}_{-0.1}\ .$$

The source and magnitude of errors associated with the $D^\pm$ and D^0 lifetimes are listed in Table III. These mean-lifetime values can be compared with the current world-average values[14] of $\tau_{D^\pm}=(9.1^{+1.1}_{-0.9})\times10^{-13}$ sec, and $\tau_{D^0}=(4.29^{+0.42}_{-0.40})\times10^{-13}$ sec.

The longest-lived neutral decay in this data has a proper flight time of 55×10^{-13} sec. The presence of this decay clearly influences the mean D^0 lifetime obtained.

TABLE III. Sources of lifetime errors in units of 10^{-13} sec.

	$D^\pm$	D^0
Ambiguous decays	±0.09	±0.13
Production model	±0.05	±0.05
Decay branching fractions	±0.17	±0.12
Error on length and impact-distance measurement	±0.25	±0.25
Λ_c^+ contamination	$^{+0.52}_{-0.0}$	
$F^\pm$ contamination	$^{+0.34}_{-0.0}$	
Statistical	±1.3	±0.9

This decay is a fully reconstructed four-prong $\bar{D}^0$ with particle identification, and therefore has a very low probability of being due to some background process. The Kolmogorov-Smirnov test[15] shows that the data sample is fully consistent with a single exponential distribution. There is no evidence to suggest the presence of a contamination due to decays of a particle having all the characteristics of the D^0 but with a different lifetime. The best estimate of the true lifetime includes this decay. For a detailed discussion of this event, see Appendix B.

C. Production mechanisms

There is direct evidence in the data of pair production of charmed mesons. Although no individual charmed-baryon decays were identified, there is indirect evidence for associated production of charmed baryons with anticharmed mesons.

1. Determination of $\sigma_{\Lambda_c^+\bar{D}X}/\sigma_{charm}$

If only pairs of charmed mesons were produced then equal numbers of D and $\bar{D}$ mesons would be expected. The observed excess of $\bar{D}$ mesons is evidence for associated production.

A total of 33 D^- and 15 D^+ decays were seen. D^0 and $\bar{D}^0$ decays were separated by identifying the charge of the K using either information from the Cherenkov counters or from fully reconstructed decays. Of the 50 neutral decays, three were identified as D^0's and 16 as $\bar{D}^0$'s. The remaining 31 neutral decays were ambiguous between D^0 and $\bar{D}^0$ interpretations. These were statistically assigned to the D^0 and $\bar{D}^0$ categories in the same ratio as the identified decays, assuming that the probability of identifying a D^0 was the same as that of identifying a $\bar{D}^0$. Adding the neutral decays to the charged decays results in totals of 23 D and 75 $\bar{D}$ mesons. The two charged/neutral ambiguous decays were added in the observed ratio of D to $\bar{D}$ decays leading to an estimated excess of 53 $\bar{D}$ decays over D decays. After weighting each event by the inverse of the detection efficiency as described in Ref. 1 and interpreting the excess as being due to $\Lambda_c^+\bar{D}X$ production, this contribution to the charm production is estimated to be

$$\frac{\sigma_{\Lambda_c^+\bar{D}X}}{\sigma_{\rm charm}}=(71\pm11\pm6)\%\ .$$

The conclusion that $\Lambda_c^+ \bar{D}X$ production is important[16] is further supported by the differences between p_{vis} of the positive and negative decays (Fig. 9).

2. Determination of $\sigma_{D\bar{D}}$

Of the 94 events which have at least one decay passing cuts, 45 were found upon examination of the high-magnification photograph to contain a second charm decay. In six events both decays pass the cuts. Background from strange-particle decays and interactions simulating charm decays is small (Sec. II D). In addition, the presence of one identified charm decay makes the interpretation of the second vertex as charmed extremely probable. K^0 and Λ decays have not been included in this sample. Three of the four one-prong decays with $l > 0.4$ mm are also compatible with $\Sigma^\pm$ or $K^\pm$ decays. The one-prong decays compatible with $\Sigma^\pm$ or $K^\pm$ interpretations and with $l > 5$ mm were not considered to be charm decays. The decay distance distribution for the 45 "shorter" decays is shown in Fig. 15. The shorter decay is that decay not passing the cuts of Sec. II B for the events where only one of the two visible decays passed the cuts.

Six events were observed containing two unambiguous neutral decays and provide direct evidence for $D\bar{D}$ pair production. In all six of these events there is only one charged track, identified as a proton in three cases, coming from the primary vertex.

An additional eight of the 45 events contain an unambiguous pair of positive and negative decays. Six of the eight have only one charged noncharmed particle coming from the primary vertex while the other two have three. The ten events containing a positive plus a neutral charm decay prefer to have extra charged pairs produced at the primary vertex (two events have no extra charged particles, six have a charged pair, and two have four extra charged particles).

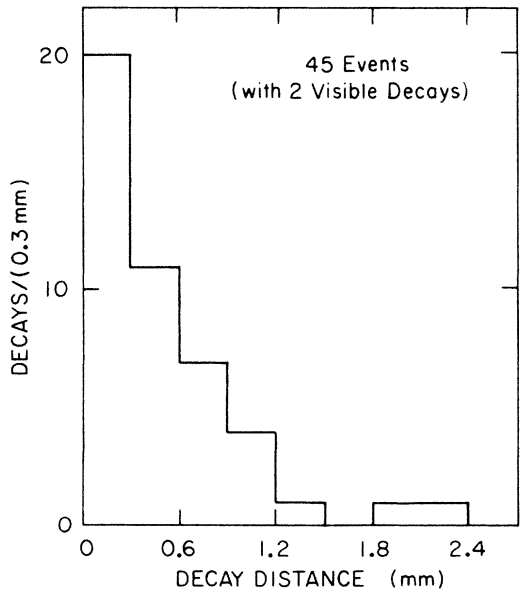

FIG. 15. Decay-length distribution for the shorter decay of events with two visible decays.

In the 49 remaining events only a single decay is visible. This can be due to several causes, these being (1) the second particle is a neutral-D meson decaying to neutral particles, (2) it is a charged charmed particle decaying into a one-prong and the kink has an angle too small to be visible, or (3) it decays at a distance which is so short that all the decay tracks appear to come from the production vertex. The threshold for visibility is less than 0.2 mm for most events but can be as large as 0.3 mm for those events with only one charged particle produced at the primary vertex, due to the possible fluctuation in the bubble density at the beginning of that particle's track.

Further selection criteria for the short decays were necessary to ensure a high and uniform detection efficiency. These decays were required to have $l > 0.5$ mm and an impact distance $d > 40$ μm. Sixteen events have one decay passing the cuts of Sec. II B and the other passing these second decay requirements. These events provide a sample from which the cross section for the production of $D\bar{D}$ pair events can be calculated. A Monte Carlo calculation (see Appendix A) of the efficiency for events containing D^+D^-, $D^0\bar{D}^0$, D^0D^-, and $\bar{D}^0D^+$ pairs to pass the double decay requirements was performed, yielding efficiencies of 19%, 15%, 17%, and 17%, respectively. A similar calculation gives an efficiency for $\Lambda_c^+ \bar{D}X$ of only 1.1% using the observed[11] Λ_c^+ lifetime of 2.3×10^{-13} sec. Using the sensitivity of Sec. II C 3, the $D\bar{D}$ efficiencies, and correcting for possible $\Lambda_c^+ \bar{D}X$ contamination the cross section for $D\bar{D}$ pair production is

$$\sigma(\gamma p \to D\bar{D}X) = 17^{+8}_{-6} \text{ nb} .$$

This independent measurement agrees with the value $18 \pm 6^{+6}_{-5}$ nb obtained using the results of the previous section and the total charm cross section (see Sec. III D 1).

3. Branching ratios for Λ_c^+ decays

(i) Λ or Σ^0 production. In the 94 charm events passing cuts there are eight visible Λ decays. All eight Λ's are consistent with coming from Λ_c^+ decays. However, the production of Λ's via $\bar{D}F^+\Lambda$ and $D\bar{D}\Lambda K$ involving more than two charmed or strange particles cannot be excluded. If the rate of Λ production in charm events were the same as for noncharm events,[10] approximately 2.3 Λ's would be expected in this sample. At the energy of this experiment the masses of the charmed particles consume a large fraction of the available phase space, suggesting that this rate is an upper limit. An improved limit of 0.4 Λ's was obtained from a study of noncharm events containing more than two observed neutral strange particles. For events containing charm this estimate is high because charmed particles are more massive than their strange counterparts. In seven of the eight events only one charm vertex is seen (six D^- and one neutral decay). The remaining event contains two visible charm decays; a short three-prong positive decay, and a $\bar{D}^0$ decay. The positive decay combined with the Λ is consistent with an unconstrained decay of a Λ_c^+, but without the Λ it is also consistent with a D^+ or F^+ decay.

The average visible momentum of the six D^- decays is 10.2 GeV/c, compared with an average of 5.4 GeV/c for

the total positive decay sample. This is consistent with the production of a fast anticharmed meson ($\bar{D}$) and a relatively slow charmed baryon (Λ_c^+). That only one of these events has a second visible charm vertex is consistent with this hypothesis and the observed[11] Λ_c^+ lifetime of about 2.3×10^{-13} sec.

Assuming the signal is caused by the decay of Λ_c^+ to Λ (or Σ^0) and using the estimate of 53 $\Lambda_c^+\bar{D}X$ events in the data sample from the results of Sec. III C 1 and the branching fraction $\Lambda\to p\pi^-$ of 0.642, the inclusive $\Lambda_c^+\to\Lambda$ branching fraction is found to be $(23\pm10)\%$. This can be compared with the present average value of[11] $(33\pm29)\%$.

(ii) $\Sigma^\pm$ production. There are five events containing a visible one-prong decay of a charged particle (four positive and one negative) at distances between 0.5 and 20 cm from the primary vertex. There is good evidence that these are charged-Σ decays. Assuming the charged-Σ momentum spectrum is similar to that observed for Λ decays, 84% of all Σ decays would occur in the range of 0.5 and 20 cm and the observed decay length distribution is consistent with that of $\Sigma^\pm$ decays having this momentum spectrum. Using observed K^0 decays from charm events, less than one $K^\pm$ decay was estimated to occur at less than 20 cm. This estimate is supported by noting that no kinks were observed in the products of the charmed decays passing cuts. For three of the five events the K^+ interpretation is Cabibbo-angle-suppressed. The $K^\pm$ background is, therefore, estimated to be less than 0.5 events.

A potential source of $\Sigma^\pm$ is due to the associated production of strange particles along with a $D\bar{D}$ pair. From measurements of photoproduced $\Sigma^\pm$ at lower energies,[17] less than one observed $\Sigma^\pm$ decay is expected to come from this source. Also, there are indications in three of the five events that the kinking track comes from a secondary vertex, which is inconsistent with this background hypothesis.

A $\Sigma^\pm$ source consistent with all the data is Λ_c^+ decay. The average visible momentum of the accompanying charm decays passing the cuts is 9.7 GeV/c, in good agreement with that measured for the events containing observed Λ decays. Assuming a background from $K^\pm$ decays of 0.5 events, correcting for the Σ decays outside $0.5<l<20$ cm and using the measured fraction of associated production, the events can be interpreted as $\Lambda_c^+\to\Sigma^\pm X$ with a branching ratio of $(10\pm5)\%$,

4. D^* production

Figure 16 shows evidence that some of the D^0 decays are themselves the product of $D^{*\pm}\to D^0\pi^\pm$ decay. This figure shows a plot of $\Delta m = m_1 - m_{\rm vis}^{\pi}$ where m_1 is the smallest effective mass formed by the D^0 decay system together with any π^+ or π^- from the primary vertex. A peak for $\Delta m < 160$ MeV/c^2 is observed. For fully reconstructed D^* decays this mass difference is 145 MeV/c^2. Even for the cases of missing neutral particles from the D^0 decay, or particle misidentification when the decay kaon is assumed to be a pion, this mass difference as shown by the solid curve in the figure is close to 145 MeV/c^2. The curve is a Monte Carlo prediction of Δm for $D^{*+}\to D^0\pi^+$ normalized to 12 events. The background to the D^* signal was estimated by calculating Δm from $D^\pm$ decays since $D^{*0}\to D^+\pi^-$ is not allowed. The background indicated by the dashed curve in the figure shows that only 2.5 events would be expected with $\Delta m < 160$ MeV/c^2. Correcting for the 29% of the D^{*+} signal predicted to fall above 160 MeV/c^2, 13.4 ± 5.0 $D^{*\pm}$ decays among the 52 possible D^0 decays passing cuts are estimated.

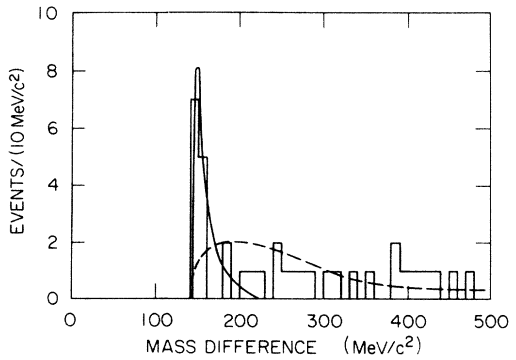

FIG. 16. Minimum mass difference between the $D^0\pi^\pm$ system and the D^0 (all tracks assumed to be pions). The solid curve is a Monte Carlo prediction for $D^{*+}\to\pi^+D^0$ (see Appendix A) and the dashed curve is the distribution expected for background (see text).

Using an estimate of 334 ± 42 charm events produced in the combined experiments (see Sec. III D 1), the branching fraction $D^{*+}\to D^0\pi^+$ of[11] $(49\pm8)\%$, and the detection-efficiency weights, the observed $D^{*\pm}$ signal corresponds to the production of 0.29 ± 0.12 $D^{*\pm}$ per charm event. This rate can be compared to 0.70 ± 0.11 $D^\pm$ per charm event.

The ratio of D^{*-}/D^{*+} in these events ($\frac{8}{4}$) can be compared to the D^-/D^+ ratio ($\frac{33}{15}$) of the complete sample. One of the 12 events with $\Delta M < 160$ MeV/c^2 has a Λ and two have a Σ^+ among the outgoing particles. In each of these cases the D^* has negative charge. Three of the D^{*-} decays into $\bar{D}^0$ have an identified K^+ among the decay products, as expected for Cabibbo-angle-allowed decays with small $(D^0$-$\bar{D}^0)$ mixing.

5. Polarization dependence

The azimuthal polarization angle ϕ of the D meson and the polarization vector, $\hat{\epsilon}$, of the photon were examined for possible correlations. The average polarization of the photon beam was calculated to be 52%. The angle ϕ is defined as

$$\phi = \arctan\left[\frac{\hat{\mathbf{k}}\times\hat{\boldsymbol{\epsilon}}\cdot\mathbf{p}_t}{\hat{\boldsymbol{\epsilon}}\cdot\mathbf{p}_t}\right],$$

where $\hat{\mathbf{k}}$ is a unit vector in the direction of the incident photon and $\mathbf{p}_t$ is the transverse momentum of the D meson with respect to the photon beam direction. Only fully reconstructed charmed decays were used so that all values of $\mathbf{p}_t$ were accurately determined. Figure 17 shows the ϕ distribution for D and $\bar{D}$ mesons. For comparison,

the corresponding distribution for π^+'s from the sample of elastically produced ρ^0 events is shown by the curve on the figure. While these ρ^0 events show a strong preference for the π^+ to be emitted in the polarization plane, the D mesons do not exhibit this behavior. There is even an apparent excess of D's for ϕ near 90°.

D. Charm-production cross section

1. The charm cross section at 20 GeV

Both pair production and associated production yield $\bar{D}$ mesons. The number of charm events produced, N_c, can be estimated by counting the $\bar{D}$'s and correcting for their detection efficiency. The details of this procedure are given in the Appendix of Ref. 1. The calculation of the efficiencies was repeated using the new projected decay length cut ($l > 0.6$ mm) which slightly reduced the detection efficiency. The dependence of the efficiency on the D momentum is shown in Fig. 18 for different lifetimes and decay multiplicities. The neutral decays were assigned to D^0 or $\bar{D}^0$ using the procedure described in Sec. III C 1. The number of D decays weighted by the inverse of the detection efficiency is given in Table IV for specific categories. Summing the contributions from $\bar{D}$ decays yields $N_c = 334 \pm 42$. The error in N_c includes the uncertainty in the number of $\bar{D}^0$'s. Using the sensitivity of Sec. II C 3, the charm cross section is found to be 62 ± 8 nb.

The value of the cross section is sensitive to several parameters (see Table V), the more important of which are

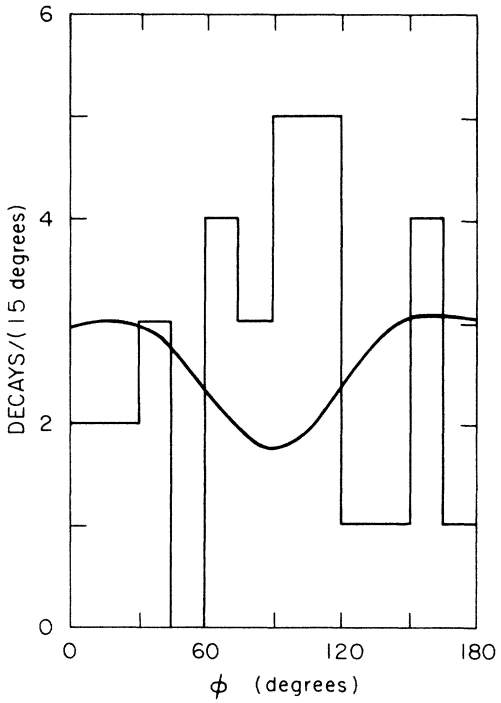

FIG. 17. The polarization-angle ϕ distribution for fully reconstructed $D/\bar{D}$ mesons. The angle ϕ is measured between the outgoing particle and the polarization vector of the photon. The curve shows the ϕ distribution for pions from elastic ρ^0 production in this experiment.

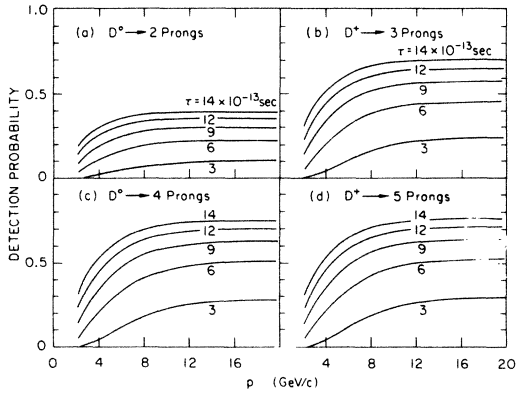

FIG. 18. Detection efficiency for various topologies and lifetimes as a function of D momentum calculated using a Monte Carlo method (see Appendix A).

the multiprong branching ratio for charged decays, τ_{D^0}, and $\tau_{D^\pm}$. The variation in the cross section due to changes in these parameters is shown in Fig. 19. Accounting for all the known sources contributing to the cross-section error,

$$\sigma_{\text{charm}} = 62 \pm 8^{+15}_{-10} \text{ nb} .$$

A model-independent lower limit to N_c can be obtained from the number of events with definite evidence for charm. This yields a value of σ_{charm} greater than 22 nb (90% confidence level).

2. Comparison of the total cross section with model predictions

Figure 20 shows the total charm photoproduction cross section at 20 GeV from this experiment together with the values obtained from two muon experiments.[18] These cross-section values from the muon experiments were corrected to reflect the most recent values of ($D \to e^+ +$anything) branching ratios of $(7.5 \pm 1.1 \pm 0.4)\%$ and $(17 \pm 1.9 \pm 0.7)\%$ for the D^0 and D^+, respectively.[19]

The curves plotted on the figure show the predictions of various models.[5] As can be seen, three of these, the photon-gluon fusion models of Babcock *et al.* and Novikov *et al.* and the vector-dominance model of Collins and Spiller are consistent with σ_{charm} measured in this experiment. However, at higher energies only the two photon-

TABLE IV. Decay categories and their weighted numbers.

Category number	Decay category	Number of decays passing cuts	Weighted numbers[a]
1	Identified D^0	3	8.4 ± 4.9
2	Identified $\bar{D}^0$	16	50.0 ± 13.6
3	Ambiguous $D^0/\bar{D}^0$	31	141.1 ± 27.1
4	Positive decays	15	80.7 ± 21.2
5	Negative decays	33	163.1 ± 28.9

[a]The two charged/neutral ambiguous decays were included in the weighted numbers as described in the text. Assigning the decays of category 3 in the ratio of the identified D^0 and $\bar{D}^0$ decays yields 29 ± 17 D^0 and 171 ± 32 $\bar{D}^0$ mesons.

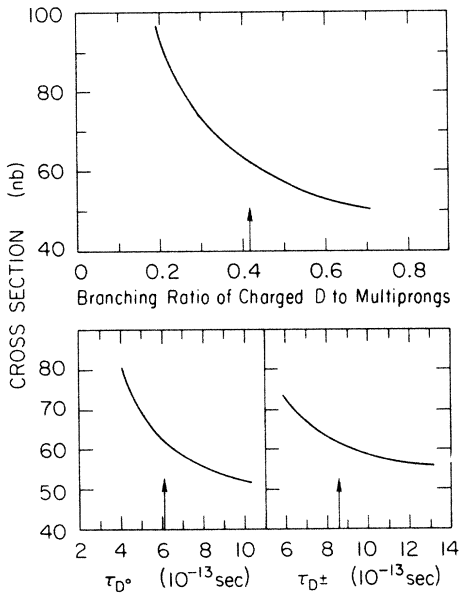

FIG. 19. Dependence of σ_{charm} on charged-D-meson multiprong branching ratio, τ_{D^0}, and $\tau_{D^\pm}$.

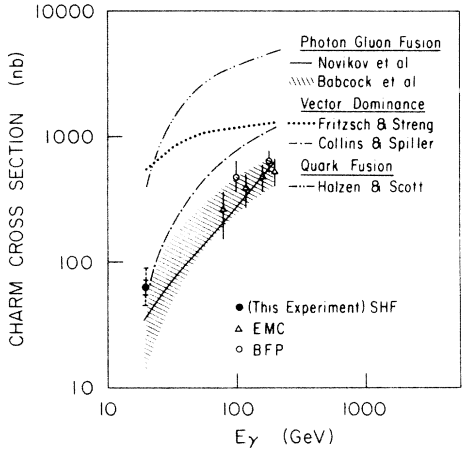

FIG. 20. Charm-production cross section as a function of energy. Data points are from this experiment and from two muon experiments. The points plotted from the muon experiments have been recalculated using the latest values of the semileptonic branching ratio obtained from the Mark III detector of $(7.5\pm1.1\pm0.4)\%$ and $(17\pm1.9\pm0.7)\%$ for the D^0 and D^+, respectively. The curves for the models of Novikov *et al.*, Fritzsch and Streng, and Halzen and Scott have been taken from their papers. In the case of the vector-dominance model of Collins and Spiller the prediction for a charmed-quark mass, m_c, of 1.86 GeV/c^2 is plotted; for lower masses the curve would be higher. The band shown for the photon-gluon fusion model of Babcock *et al.* is bounded by values of $m_c=1.5$ GeV/c^2 (upper bound) and $m_c=1.86$ GeV/c^2 (lower bound).

gluon fusion models are consistent with the muon data. In order to show the dependence of the model predictions on the assumed mass of the charmed quark, m_c, a band was plotted in the case of the model of Babcock *et al.* bounded by taking $m_c=1.86$ GeV/c^2 (lower bound) and $m_c=1.5$ GeV/c^2 (upper bound). In the case of the model of Collins and Spiller only the curve corresponding to $m_c=1.86$ GeV/c^2 was plotted, lower values of m_c yield higher cross sections.

In conclusion, the photon-gluon fusion models of Novikov *et al.* and Babcock *et al.* describe the total-cross-section data well. The quark fusion model of Halzen and Scott and the vector-dominance model of Fritzsch and Streng clearly predict much larger cross sections than are observed, while the vector-dominance model of Collins and Spiller, although compatible with this experiment's measurement, predicts higher cross sections than are observed by the two muon experiments.

IV. CONCLUSIONS

In the BC75 exposure of the SLAC Hybrid Facility to a 20-GeV photon beam, 71 events were observed to contain the decays of charmed particles meeting stringent selection criteria. The data from this and a previous experiment at the SHF (BC72/73) were found to be consistent and were, therefore, combined yielding a total of 136 events. After imposing rigorous cuts on the data, 100 charmed-particle decays remained contained in 94 events. The efficiency for finding decays in the region above the cuts was measured to be high and uniform as a function of decay distance. Charged and neutral decays were treated in exactly the same way.

Using the 50 neutral, 48 charged, and 2 charged/neutral ambiguous decays, remaining after cuts, the lifetimes are measured to be:

$$\tau_{D^\pm}=(8.6\pm1.3^{+0.7}_{-0.3})\times10^{-13}\text{ sec},$$

$$\tau_{D^0}=(6.1\pm0.9\pm0.3)\times10^{-13}\text{ sec},$$

TABLE V. Various sources contributing to the total-charm-cross-section error.

	Contribution to positive uncertainty in $\Delta\sigma_c$ (nb)	Contribution to negative uncertainty in $\Delta\sigma_c$ (nb)
Statistical errors	7.8	7.8
Uncertainty in branching ratio of charged decays to multiprongs	9.3	5.8
Uncertainty in branching ratio of neutral decays to multiprongs	3.8	3.3
Uncertainty in τ_{D^0}	8.0	4.6
Uncertainty in $\tau_{D^\pm}$	5.2	3.7
Uncertainty in sensitivity	4.6	3.9

and the lifetime ratio is

$$\frac{\tau_{D^\pm}}{\tau_{D^0}} = 1.4 \pm 0.3^{+0.2}_{-0.1} .$$

Firm evidence for production of D and $\bar{D}$ mesons via both pair ($D\bar{D}X$) production and associated ($\bar{D}\Lambda_c^+ X$) production was found. There is no evidence for F decays in the data, and no significant limits can be placed on F production by this experiment. The fraction of associated production is

$$\frac{\sigma_{\Lambda_c \bar{D} X}}{\sigma_{\text{charm}}} = (71 \pm 11 \pm 6)\% ,$$

and the total charm cross section is

$$\sigma_{\text{charm}} = 62 \pm 8^{+15}_{-10} \text{ nb} .$$

Using $D^{*\pm} \to D^0 \pi^\pm$, it was found that there are 0.29 ± 0.12 $D^{*\pm}$ mesons per charm event. Branching fractions for Λ_c^+ were measured to be $(23 \pm 10)\%$ for $(\Lambda_c^+ \to \Lambda^0 X^+)$ and $(10 \pm 5)\%$ for $(\Lambda_c^+ \to \Sigma^\pm X)$.

ACKNOWLEDGMENTS

We wish to thank Professor W. K. H. Panofsky, the recently retired director of SLAC, for his continued encouragement and support throughout the span of this experiment. We thank the SLAC bubble-chamber crew for their dedication and performance under difficult bubble-chamber operating conditions, particularly for their work on the high-resolution camera. We are especially indebted to the film scanners for their meticulous efforts in finding the events. We thank the groups at Duke University, Florida State University, KEK Japan, MIT, Nara Women's University Japan, Technion—Israel Institute of Technology, University of Tel Aviv, and the Wiezmann Institute for their permission to use the data from the previous experiment. We also thank Steve Tether and Dick Yamamoto of MIT and Avi Yagil of Technion for their assistance in collecting the data. This work was supported in part by the Department of Energy, under Contract No. DE-AC03-76SF00515, the Japan-U.S. Cooperative Research Project on High Energy Physics under the Japanese Ministry of Education, Science and Culture; the UK Science and Engineering Research Council; and the U.S. National Science Foundation.

APPENDIX A: MONTE CARLO SIMULATION

Monte Carlo calculations were used to obtain efficiencies for detecting charmed-particle decays passing the cuts of Sec. II B, estimating parameters used in the calculation of the charmed-particle lifetimes (Sec. III B) and studying possible biases of the experimental technique. Two independent Monte Carlo simulation programs using different assumptions about the production mechanism were used. The sensitivity of the results to the assumed production mechanism is small.

1. Charm-decay parameters

The two programs used measured $D^\pm$ and D^0 inclusive and exclusive final states as input.[11] All D decay distributions were assumed to be isotropic in the D rest frame.

Provided the charmed baryon has a short lifetime (i.e., approximately 2.3×10^{-13} sec) the predictions from the Monte Carlo are very insensitive to Λ_c^+ decay characteristics.

2. Pair production and associated production

The following final states were generated: $D\bar{D}N(n\pi)$, $D^*\bar{D}N(n\pi)$, $\bar{D}^*DN(n\pi)$, $D^*\bar{D}^*N(n\pi)$, $\Lambda_c^+\bar{D}(n\pi)$, $\bar{D}^*\Lambda_c^+(n\pi)$, and $\bar{D}\Sigma_c^{++}(n\pi)$, where $n = 0,1,2,\ldots$. The extra pions were produced at either the nucleon or meson vertex.

All possible charge combinations were generated according to a simple statistical model. The invariant four-momentum transfer squared, assumed to be distributed exponentially between the photon and meson system, was chosen for each reaction so as to reproduce the observed momentum spectrum.

3. Monte Carlo results

The curves in Figs. 8, 10, 13, 16, 18, and 19 were calculated using the lifetimes and cross sections found in this experiment.

APPENDIX B: THE LONGEST-LIVED NEUTRAL DECAY

The event containing the longest-lived neutral decay in the data is shown in Fig. 21, and some of its characteris-

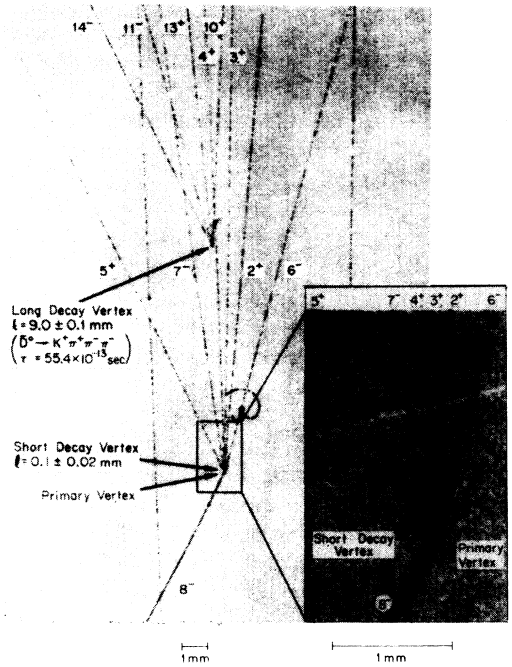

FIG. 21. Photograph of the event containing the longest-lived neutral D meson found in this experiment. The picture was taken by the high-resolution camera. Inset shows enlargement of region around the primary vertex and short-decay vertex. The positions of the primary and short-decay vertices were determined by measurement. The event is fully compatible with the decays of two charmed particles, the decay at 9 mm being a $\bar{D}^0 \to K^+\pi^+\pi^-\pi^-$ with a proper flight time of 55.4×10^{-13} sec. Details of the event are discussed in Appendix B.

TABLE VI. General characteristics of the event containing the longest-lived D^0. For track numbering, see Fig. 21.

Track No.	Charge	Momentum MeV/c	Identity	Identified by	Vertex
6	−	489±6	$e/\mu/\pi$	Ionization	Primary
3	+	4017±48			Primary
4	+	382±4	$e/\mu/\pi$	Ionization	or
7	−	431±4	$e/\mu/\pi$	Ionization	short decay
2	+	3030±330	K^+/Σ^+	Decay	
5	+	1072±12	not proton	Ionization	Short decay
8	−	65±2	π	Range	
10	+	5452±56	K/p	Cherenkov	
11	−	599±6	$e/\mu/\pi$	Ionization	Long
13	+	3694±33	$e/\mu/\pi$	Cherenkov	decay
14	−	466±4	$e/\mu/\pi$	Ionization	
15	0	574±53	γ	Lead glass	Any

tics are given in Table VI. It contains two decays: a short decay at 0.10±0.02 mm into at least two charged particles and a long neutral decay into four charged particles at a distance of 9.0±0.1 mm from the production vertex.

Close inspection of the high-resolution film led to the conclusion that particles 5^+ and 8^- definitely came from the short decay vertex and that particle 2^+ probably did. Tracks 8^-, 5^+, and 2^+, projected back, miss the production vertex by 52±7, 42±7, and 20±6 μm, respectively. Tracks 3^+,4^+,7^- are ambiguous between the primary vertex and the short decay vertex, while track 6^- clearly comes from the primary vertex. Particle 2^+ underwent a one-prong decay after 3.1 cm (off the photograph of Fig. 21) and is identified as a K^+ or Σ^+. There is no indication of a recoil proton stub at the short decay vertex. For those particles definitely coming from the short vertex, particle 5 can be e^+, μ^+, π^+, or K^+ while particle 8^- is identified as a pion by range. The minimum mass of this decaying particle is $m(e^+\pi^-)=652\pm5$ MeV/c^2 ruling out all strange-particle-decay interpretations. The short decay, however, is fully compatible with being a charmed-particle decay.

The long decay at 9 mm from the production vertex has four charged particles and its decay vertex is clearly separated from all other tracks. The identities of the charged particles are given in Table VI. The invariant mass of the $K^+\pi^+\pi^-\pi^-$ system is 1862±8 MeV/c^+ and is consistent with the accepted $\bar{D}^0$ mass. Also, the decay shows no transverse momentum imbalance (the momentum vector of the four decay particles projected onto the film plane has a component transverse to its line of flight of 65±100 MeV/c). Thus, all the evidence is fully consistent with the decay of a 10.10±0.06 GeV/c $\bar{D}^0$ into $K^+\pi^+\pi^-\pi^-$. The proper flight time is calculated to be $(55.4\pm0.7)\times10^{-13}$ sec.

All possible sources of background which could simulate a constrained four-prong $\bar{D}^0$ decay (within 5σ of the D^0 mass and within 15 mm of the production vertex which is the maximum scanning length in these experiments) were examined.

It should be noted that the four-prong decay cannot be due to the interaction of any neutral particle on a proton, since the minimum range of the recoil proton is 1.3 cm and it would be seen. Also this decay cannot be simulated by the decay $K_L^0\to\pi^+\pi^-\pi^0$ with a Dalitz decay of the π^0 since there is no possible e^+e^- mass less than 135 MeV/c, particle 10^+ is not an e or a π, and $m(\pi^+\pi^-e^+e^-)\gg m_K$.

The only possible background is that due to an interaction of a neutral particle on a deuteron present in the liquid hydrogen resulting in a four-prong interaction with an unseen spectator proton; this configuration simulates a decay. In the background calculation it was required that the mass of the four-body system be within 5σ of the $\bar{D}^0$ mass. In the case of a neutron interaction this mass was required to be within 5σ of a $p\pi^+\pi^-\pi^-$ mass of 2159 MeV/c^2 (which would be obtained if a proton were substituted for the K^+). The existence of the short decay in the event was taken into account. The joint probability P that this experiment would contain a background event simulating the two charmed-particle decays was calculat-

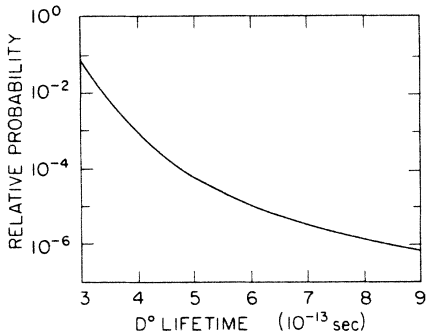

FIG. 22. Upper limit to the relative probability that the event containing the longest-lived $\bar{D}^0$ decay is due to background compared to the charmed-particle-decay interpretation.

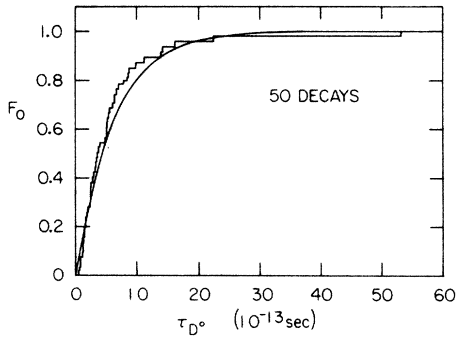

FIG. 23. The Kolmogorov-Smirnov test comparing observed cumulative distribution function of the data sample and the theoretical cumulative distribution function.

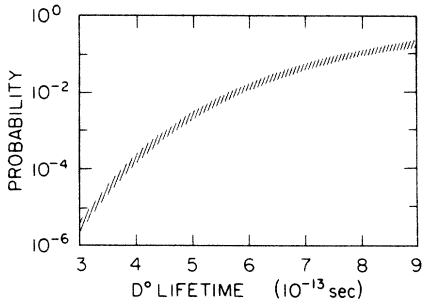

FIG. 24. Probability that an experiment of the size of the combined BC72/73 and BC75 exposures would contain an acceptable $D^0/\bar{D}^0$ with proper flight time $\tau > 55\times10^{-13}$ sec as a function of D^0 lifetime. Shaded area represents the uncertainty ($\pm1\sigma$) in the calculated number of $D^0/\bar{D}^0$ produced.

ed. Four possible sources of background were considered.

(i) A photon interaction with a short decay (not of a charmed particle) followed by a secondary interaction of a K^0 from the production vertex with a deuteron in the liquid hydrogen, $K^0d\rightarrow K^+\pi^+\pi^-\pi^-(\pi^0)n(p_s)$ ($P<6\times10^{-10}$).

(ii) Primary and short decay vertices as in (i) and a secondary interaction of a neutron from the production vertex with a deuteron in the liquid hydrogen, $nd\rightarrow p\pi^+\pi^-\pi^-(\pi^0)n(p_s)$ ($P<2\times10^{-10}$).

(iii) Two independent photon interactions, one giving the production and short decay vertex and the other giving the four-prong vertex 9 mm downstream ($P<0.3\times10^{-10}$).

(iv) Production of a charm-anticharm pair with the long four-prong decay simulated by a secondary K^0 (from the subsequent decay of either of the two charmed particles) interacting with a deuteron in the liquid hydrogen. In this hypothesis the short visible decay at 0.1 mm is then from the decay of one of the charmed particles produced and the other charm decay is not visible.

Background source (iv) has the highest probability in this experiment. The expression used to obtain the probability that this experiment contains a secondary interaction on a deuteron simulating a $\bar{D}^0$ of this type within 15 mm of the production vertex is

$$P = N_{\text{charm}} f_1 f_2 f_3 f_4 \left[\frac{15}{l}\right] f_5 ,$$

where N_{charm} is the number of the charm-anticharm particle pairs in the whole film. In Sec. III D 1, N_{charm} is estimated to be 334 ± 42. (This estimate is only weakly dependent on the charm lifetime.) f_1 is the number of K^0's per charmed pair produced with momentum larger than the minimum necessary to generate the required mass ($=0.4$), f_2 is the fraction of interactions on deuterons in which the spectator proton is not seen on the high-resolution photograph ($=\frac{1}{3}$), f_3 is the fraction of deuteron molecules in the liquid hydrogen ($=1.5/10000$) (measurements within this experiment are consistent with this natural frequency), f_4 is the fraction of the $(K^+\pi^+\pi^-\pi^-)$ invariant-mass plot within $5\sigma(\pm40$ MeV/c^2) of the D^0 mass ($=\frac{1}{10}$, this being averaged over the K^0 momentum spectrum above threshold), l/f_3 is the mean free path in millimeters for a K^0 to interact on a neutron giving a $K^+\pi^+\pi^-\pi^-n(\pi^0)$ final state, averaged over the K^0 momentum spectrum. The cross section for the above reactions was estimated to be <2 mb. From this $l/f_3 > 130000\times10000/1.5$ ($=0.87\times10^9$). f_5 is the fraction of the cross section for the above reactions for which the p_T imbalance would not have been clearly observed ($=\frac{1}{4}$). The probability P that in this experiment the long decay comes from this background source is less than 1.7×10^{-8}.

The upper limit to the relative probability that the event is due to background compared to the charm interpretation is shown in Fig. 22. In this calculation it was required that the $D^0/\bar{D}^0$ decay into $K^{\mp}\pi^{\pm}\pi^+\pi^-$ (with a 7.1% branching ratio)[14] and decay after 55×10^{-13} sec. It can be seen that the relative probability is very small for the lifetime of this experiment, $\tau_{D^0}=6.1\times10^{-13}$ sec, and is small even for considerably shorter lifetimes.

In order to estimate the probability that the neutral decays are a sample from a single exponential distribution the Kolmogorov-Smirnov test[15] was applied. This is a well-defined procedure for testing the goodness of fit of a theoretical distribution to a set of independent observations. It involves a comparison between the observed cumulative distribution function of the data sample and the theoretical cumulative distribution function. For small samples it is superior to the χ^2 test. Figure 23 shows the cumulative distribution for the observed neutral decays together with that expected for an exponential decay distribution having a mean lifetime of 6.1×10^{-13} sec. The maximum deviation is 0.095. This was compared with the distribution of deviations in a Monte Carlo simulation and it was found that only 50% of the simulated 50-event experiments have a smaller maximum deviation. Therefore, the distribution is fully compatible with a single exponential distribution.

Figure 24 shows the probability that an experiment of the size of the combined BC72/73 and BC75 ones would contain an acceptable $D^0/\bar{D}^0$ with proper flight time $>55\times10^{-13}$ sec as a function of D^0 lifetime. The calculation of the probability took into account the fact that the total number of $D^0/\bar{D}^0$ produced, estimated from the observed number of $D^0/\bar{D}^0$, depends on the lifetime. The shaded region indicates the uncertainty in this number

($\pm 1\sigma$). For the lifetime of 6.1×10^{-13} sec, this probability is 2.0%. The probability decreases rapidly with decreasing lifetime and is 6×10^{-4} for the Particle Data Group[11] value of $4.4^{+0.8}_{-0.6}\times10^{-13}$ sec.

In conclusion, a γp interaction containing two decays was found and it is fully compatible with the decays of two charmed particles. The longer-lived decay is a $\bar{D}^0\to K^+\pi^+\pi^-\pi^-$ with a proper flight time of 55.4×10^{-13} sec. The probability for an event having these characteristics coming from background sources is extremely small (less than 1 in 6×10^7 experiments of this size). In addition, the neutral charm decays including this long-lived $\bar{D}^0$ have a distribution of proper flight times fully consistent with a single exponential distribution.

---

*Present address: CERN, Geneva, Switzerland.

†On leave from Technion—Israel Institute of Technology, Haifa, Israel.

‡Present address: The Analytical Sciences Corporation, Reading, MA 01867.

§Present address: Fermilab, Batavia, IL 60510.

**Present address; Langton EPS, London, England.

[1]K. Abe *et al.* (SLAC Hybrid Facility Photon Collaboration), Phys. Rev. D **30**, 1 (1984).

[2]M. K. Gaillard, B. W. Lee, and J. L. Rosner, Rev. Mod. Phys. **47**, 277 (1975); J. Ellis, M. K. Gaillard, and D. V. Nanopoulos, Nucl. Phys. **B100**, 313 (1975).

[3]N. Ushida *et al.*, Phys. Rev. Lett. **45**, 1049 (1980); **45**, 1053 (1980); W. Bacino *et al.*, *ibid.* **45**, 329 (1980); R. M. Schindler *et al.*, Phys. Rev. D **24**, 78 (1981).

[4]M. Bander *et al.*, Phys. Rev. Lett. **44**, 7 (1980); H. Fritzsch and P. Minkowski, Phys. Lett. **90B**, 455 (1980).

[5]F. Halzen and D. M. Scott, Phys. Lett. **72B**, 404 (1978); H. Fritzsch and K. M. Streng, *ibid.* **72B**, 385 (1978); J. Babcock *et al.*, Phys. Rev. D **18**, 162 (1978); V. A. Novikov *et al.*, Nucl. Phys. **B136**, 125 (1978); P. D. B. Collins and T. P. Spiller, Durham University Theory Reports Nos. 84/22 and 84/26, 1984 (unpublished).

[6]J. D. Ferrie and R. C. Field, Nucl. Instrum. Methods **221**, 330 (1984).

[7]A. V. Bevan *et al.*, IEEE Trans. Nucl. Sci. **NS-32**, 1313 (1985).

[8]D. A. Evans and W. H. Barkas, Nucl. Instrum. Methods **56**, 289 (1967).

[9]H. Geiger and A. Werner, Z. Phys. **21**, 187 (1924).

[10]K. Abe *et al.*, Phys. Rev. D **29**, 1877 (1984).

[11]Particle Data Group, Rev. Mod. Phys. **56**, S1 (1984).

[12]B. Franek, Rutherford Appleton Laboratory Report No. RAL85-026, 1985 (unpublished).

[13]Using the method of Ref. 1, based on a maximum-likelihood calculation the result for the present data sample (ignoring the ambiguous decays) is a charged lifetime of $(7.9^{+1.3}_{-1.2})\times10^{-13}$ sec and a neutral lifetime of $(6.0^{+0.9}_{-0.8})\times10^{-13}$ sec (statistical errors only). Results obtained by the two methods are therefore fully compatible.

[14]R. Klanner, in *Proceedings of the 22nd International Conference on High Energy Physics, Leipzig, 1984,* edited by A. Meyer and E. Wieczorek (Academie der Wissenschaften der DDR, Zeuthen, DDR, 1984).

[15]A. G. Frodesen, O. Skjeggestad, and H. Tofte, *Probability and Statistics in Particle Physics* (Columbia University Press, New York, 1979).

[16]In BC72/73 (Ref. 1), the fraction of $\Lambda_c^+\bar{D}X$ production was calculated using a different method to be (35 ± 20)%. In addition to the excess of $\bar{D}$ mesons, this method used the excess of visible Λ's, the production of $D^0\bar{D}^0X$ events and events in which both decays passed the cuts. For this calculation several assumptions were made. These include the branching ratio of Λ_c^+ to Λ (assumed to be 50%), the fraction of $D\bar{D}$ pair production which is $D^0\bar{D}^0$ (assumed to be $\frac{3}{14}$) and the Λ_c^+ detection efficiency (which depends on the Λ_c^+ lifetime, momentum spectrum, and branching ratios). That result is very sensitive to these assumptions. For example, if the Λ_c^+ to Λ branching ratio presented in Sec. III C 3 had been used the estimate for the $\Lambda_c^+\bar{D}X$ fraction obtained from the excess of Λ decays would have increased by a factor of 2. The method used in Sec. III C 1 has fewer assumptions and a smaller uncertainty. When the BC72/73 events are treated in the same way as those found in BC75 and the method of analysis described in Sec. III C 1 is used, a result of (68 ± 18)% is obtained, quite consistent with the present value.

[17]R. Erbe *et al.*, Phys. Rev. **188**, 2060 (1969).

[18]J. J. Aubert *et al.*, Nucl. Phys. **B213**, 31 (1983); A. R. Clark *et al.*, Phys. Rev. Lett. **45**, 682 (1980).

[19]R. M. Baltrusaitis *et al.*, Phys. Rev. Lett. **54**, 1976 (1985).

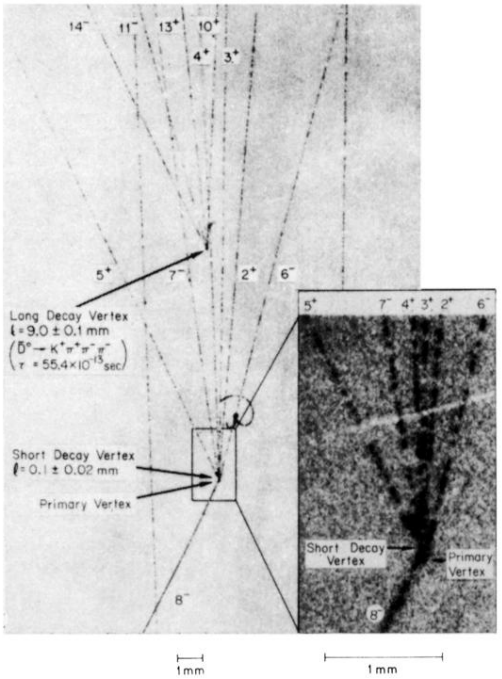

FIG. 21. Photograph of the event containing the longest-lived neutral D meson found in this experiment. The picture was taken by the high-resolution camera. Inset shows enlargement of region around the primary vertex and short-decay vertex. The positions of the primary and short-decay vertices were determined by measurement. The event is fully compatible with the decays of two charmed particles, the decay at 9 mm being a $\overline{D}^0 \rightarrow K^+\pi^+\pi^-\pi^-$ with a proper flight time of 55.4×10^{-13} sec. Details of the event are discussed in Appendix B.